PERGAMON

International Journal of Multiphase Flow 26 (2000) 1645–1673

International Journal of Multiphase Flow

www.elsevier.com/locate/ijmulflow

Wall and interfacial shear stress in pressure driven two-phase laminar stratified pipe flow

D. Biberg*, G. Halvorsen

Institute for Energy Technology, P.O. Box 40, N-2027 Kjeller, Norway

Received 26 November 1997; received in revised form 2 November 1999

Abstract

Two-phase pressure driven laminar stratified pipe flow is studied with emphasis on the wall and interfacial shear stresses. The basic solution of the Navier–Stokes equations is recast into a simpler form, alleviating physical interpretation and constituting a convenient basis for further developments. Utilizing two-phase symmetry facilitates writing the velocity field for each phase as one generic expression, which is then split into a linear combination of two terms. The first term equals the single-phase free surface flow of either phase due to the given driving forces. The second term links the phases together and represents the shear flow given by the interfacial drag from the opposite phase. The corresponding expression for the interfacial shear stress now emerges naturally as part of the solution of the boundary value problem. The wall shear stresses are obtained by formal differentiation. The limiting behaviour of the wall and interfacial shear stresses in the triple points, where the fluid–fluid interface meets the pipe wall, is obtained by application of residue calculus. Surprisingly, it proves possible to integrate out the Fourier integrals in the expressions for the *mean* wall and interfacial shear stresses. The expressions for the mean wall shear stresses are demonstrated to be equivalent to the fluid momentum balances, thus confirming consistency. The new and remarkably simple closed form expression for the mean interfacial shear stress, however, represents the local solution of the boundary value problem at the interface, not obtainable from a regular force balance. It thus complements the momentum balances, facilitating a simple computation of the exact general solution for the mean wall and interfacial shear stresses for a given holdup and pressure drop in a given pipe containing a given pair of fluids. The equation system developed here forms the basis for the inversion of the laminar stratified pipe flow problem in terms of flow rates. The corresponding, however, considerably more transparent, channel flow solution is utilized as a guide to the pipe flow problem.

Keywords: Two-phase; Laminar; Stratified; Pipe flow; Shear stress

* Corresponding author.

0301-9322/00/$ - see front matter
PII: S0301-9322(99)00109-3

1. Introduction

This article is concerned with the study of the analytic solution for two-phase laminar stratified pipe flow in terms of holdup and pressure drop. Special emphasis is put on the expressions for the wall and interfacial shear stress. It covers the basic solutions for the velocity field, the corresponding wall and interfacial shear stress distributions and their mean values. The limiting behaviour of the shear stresses in the triple points, where the fluid–fluid interface meets the pipe wall is also given. The equations constitute the basis for the inversion of the laminar pipe flow problem in terms of flow rates, i.e. the correct formulation for holdup and pressure drop computations, and thus also the natural formulation from an engineering point of view. The actual inversion of the laminar flow problem will, however, be addressed later.

Thestudy of two-phase laminar stratified pipe flow was launched as a fundamental approach for obtaining a better theoretical basis for the development of 1D flow models. Laminar flow, of course, constitutes a particularly simple special case in that an exact solution of the Navier–Stokes equations is possible. It was believed to be valuable to carefully examine, and understand, this solution before moving on to the more relevant, however, substantially more complicated *turbulent* flow case. The intention was to look for principles which might carry over to turbulent flows. In 1D turbulent flow, the expressions for the mean wall and interfacial shear stresses constitute the basic closure laws, which must be determined in order to predict the flow. It was thus natural to focus on the corresponding expressions in laminar flow. The analysis turned out to reveal some up until now unpublished results, which will be presented here. Turbulent flows will not be considered (thus avoiding any confusion with the turbulent flow case). Some interesting results concerning the application of laminar flow theory to turbulent flows may, however, be found in Biberg (1999a).

Many workers have studied the analytic solution for two-phase laminar stratified pipe flow. The earliest basic solution of the Navier–Stokes equations known to the authors, i.e. the solution for the velocity field in terms of holdup and pressure drop, is given by Teletov (1946) who solved the problem using Poisson integrals. Later Semenov and Tochigin (1961) developed the solution in terms of Fourier integrals. They also obtained the corresponding expressions for the mean velocities by integration. Rosant (1986) obtained an alternative solution in terms of Fredholm integrals. Considering horizontal flow only, and applying Fourier integrals, Bentwich (1964) solved the more complicated problem in which the interface is assumed to have the *circular* shape given by an isoline in the bipolar coordinate system. Depending on a single parameter, the interface in Bentwich's solution may assume all stages between a circular-cylinder (annular flow) and an arc-segment of a circle with a possible infinite radius corresponding to a flat interface. The physical mechanism determining the radii of the surface curvature was not considered. The basic solutions for the velocity field as given by Bentwich, Semenov and Tochigin coincide in the flat interface horizontal flow case. Brauner et al. (1996a) derived the expressions for the wall and interfacial shear stress from Bentwich's solution, by formal differentiation.[1] They studied the

[1] Brauner et al.'s claim (pp. 104 and 120) that (Bentwich's, 1964) solution is inapplicable in practical computations due to singularities of the integrand is based on a misconception — there are no singularities in the integrand. In fact, disregarding some minor formal differences, the solution considered by Brauner et al. is identical to Bentwich's solution.

limiting behaviour of the shear stress in the triple points, where the fluid–fluid interface meets the pipe wall, mainly by numerical experimentation. An analytic result was, however, obtained in the special case of equal phase's holdup. Brauner et al. (1996b) applied Bentwich's solution to study the effect of surface curvature associated with the action of surface tension forces in small-scale systems. They determined the (constant) radius of interfacial curvature by application of an energy argument. (The actual *shape* of the interface is not determined in this study. It is simply a priori assumed to be given by an arc segment of a circle.)

Other relevant analytic studies of two-phase laminar–laminar stratified pipe flow are given by Packham and Shail (1971), Ranger and Davis (1979) and Lightstone and Chang (1991). Numerical solutions are given by Charles and Redberger (1962), Gemmell and Epstein (1962), Yu and Sparrow (1967) and Masliyah and Shook (1978). The analytic solution for the related *rectangular* duct flow problem is considered by Tang and Himmelblau (1963) and Charles and Lilleleht (1965). The channel flow problem is studied in e.g. Coutris et al. (1989). The solution for a liquid in laminar flow in the bottom of a pipe, subject to a *constant* prescribed interfacial shear stress distribution, approximating the action of a turbulent gas in the upper portion of the pipe, is also relevant for the present study, see Biberg (1999b).

We will only consider flows with a flat interface here. The effect of pipe inclination, which is connected to a number of interesting two-phase flow phenomena such as e.g. the possibility of backflow in either phase, will, however, be accounted for. Our interest in the two-phase laminar stratified pipe flow is of a purely analytical nature. No comparisons with experiments are involved. It is, however, generally accepted that the solution of the Navier–Stokes equations agrees closely with reality provided that the underlying premises are fulfilled. The validity of laminar flow theory to two-phase flows has been experimentally verified by Yu and Sparrow (1969) in a study of oil/water flow in a horizontal 9/16 in. high and 9/8 in. wide rectangular duct. Interestingly, they found the flow and pressure drop to be insensitive to the presence of very small interfacial waves, thus extending the applicability of the non-wavy interface assumption in this case. It is beyond the scope of this work to rigorously establish for which parameter range two-phase flat interface laminar stratified pipe flow is physically realizable. However, it is known that the transition to turbulent flow, given by a Reynolds number of approximately 2000 in single-phase pipe flow, seems to take place at a somewhat lower Reynolds number in two-phase flow. The enhanced transition is probably caused by interfacial instabilities leading to the formation of interfacial waves. Interfacial curvature connected to viscous effects may be observed in low density difference systems, see e.g. Joseph (1984). Similarly, surface tension forces may cause surface curvature in small scale systems (capillary tubes). In a large scale system with a certain density difference, however, the fluid–fluid interface will always be flat (horizontal), except perhaps for a narrow region in the vicinity of the pipe wall, where surface tension forces influence the interface to wall contact angle.

2. The boundary value problem

The boundary value problem for two-phase laminar stratified pipe flow is defined in Fig. 1. A less dense fluid g is flowing on top of a more dense fluid l. The fluids $f = g$ and l are

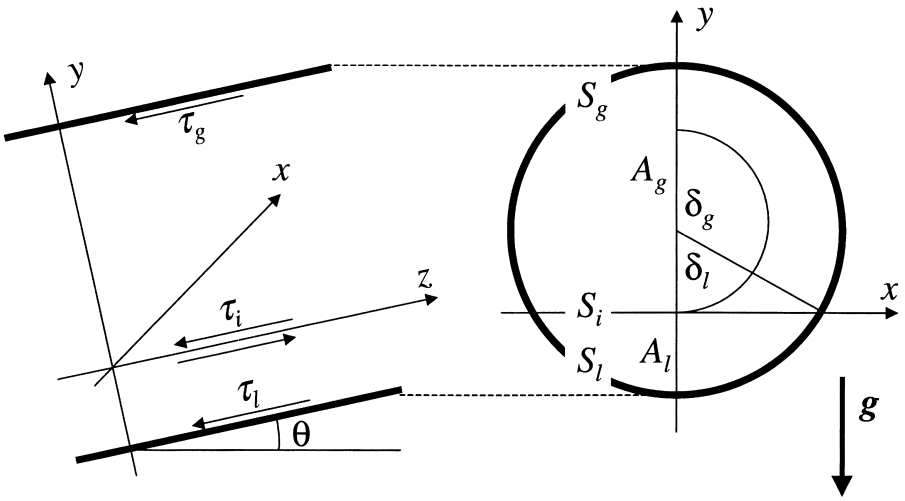

Fig. 1. Definition sketch.

assumed to be immiscible, homogeneous, incompressible and Newtonian, with constant viscosities η_f and densities ρ_f. The pipe inclination to the horizontal is θ. The flow is referred to a Cartesian coordinate system (x, y, z), orientated with the z-axis pointing in the direction of flow and the fluid–fluid interface i defined by $y = 0$.

The flow is assumed to be parallel and steady state i.e. with phase velocity vectors given by $\mathbf{U}_f = u_f(x, y)\mathbf{i}_z$. The y-components of the Navier–Stokes equations for each phase thus reduce to

$$\frac{\partial p}{\partial y} + \rho_f g \cos\theta = 0 \tag{1}$$

Differentiation of Eq. (1) with respect to z yields

$$\frac{\partial}{\partial z}\left(\frac{\partial p}{\partial y}\right) = \frac{\partial}{\partial y}\left(\frac{\partial p}{\partial z}\right) = 0$$

which shows that the pressure gradient in the z-direction in each phase is constant in a vertical cross section. Since the pressure at the interface must be equal in each phase for all z, the pressure gradient must also be equal in each phase. The pressure in a cross section of the pipe, however, varies hydrostatically, as may be confirmed by integration of Eq. (1). The z-components of the Navier–Stokes equations are given by

$$\nabla^2 u_f = \frac{B_f}{\eta_f} \quad \text{in } A_f \tag{2}$$

in which

$$B_f = \frac{\partial p}{\partial z} + \rho_f g \sin\theta \tag{3}$$

where $-B_f$ is the constant driving force in phase f in the direction of flow and A_f is the corresponding flow area occupied by fluid f and enclosed by the corresponding wall wetted perimeter S_f and the fluid–fluid interface S_i. The boundary conditions are the no-slip conditions on the pipe wall and interface, given by

$$u_f = 0|_{S_f} \tag{4}$$

and

$$u_g = u_l|_{S_i} \tag{5}$$

respectively, and the conditions for continuous shear stress across the interface, given by

$$\eta_f \frac{\partial u_f}{\partial y}\bigg|_{S_i} = \tau_i \tag{6}$$

in which τ_i denotes the interfacial shear stress distribution.

3. Solving the boundary value problem

In the following, corresponding equations for the fluids $f = g$ and l will often be written as a single expression for fluid f. This saves space. More importantly, however, it emphasizes the natural two-phase symmetry of the boundary value problem. We apply the notation $\pm$ or $\mp$ in order to account for the occurrence of opposite signs in corresponding terms. The upper and lower signs are to be associated with the less and more dense fluids $f = g$ and l, respectively, flowing in the upper and lower portions of the pipe. We now seek a solution of the boundary value problem (2)–(6) in the form

$$u_f = u_f^p + \phi_f \tag{7}$$

in which the Hagen–Poiseuille solution for single-phase pipe flow of phase f, given by

$$u_f^p = -\frac{B_f}{4\eta_f}(R^2 - r^2) \tag{8}$$

is used as a particular solution, and ϕ_f are the homogeneous solutions. In the coordinate system defined in Fig. 1, we have $r^2 = x^2 + (y \pm R\cos\delta_f)^2$, where R is the pipe inner radius. The wetted angles δ_f are interrelated by $\delta_g + \delta_l = \pi$. The one-to-one relation between δ_f and the corresponding phase fractions $\epsilon_f = A_f/A$, may be obtained by application of simple trigonometry to Fig. 1, yielding

$$\epsilon_f = \frac{1}{\pi}\left(\delta_f - \frac{1}{2}\sin 2\delta_f\right) \tag{9}$$

There are, however, no known *simple* solutions (9) for δ_f in terms of ϵ_f, see Biberg (1999c). We will therefore for simplicity, work with the wetted angles δ_f as a substitute for the more

commonly used phase fractions ϵ_f. We will also frequently refer to expressions depending on δ_f as being holdup dependent, since a given holdup ϵ_l corresponds to the void fraction $\epsilon_g = 1 - \epsilon_l$, and thus (implicitly) determines δ_f through Eq. (9).

The bipolar (ξ, ζ) coordinate system is the natural orthogonal coordinate system for the stratified flow geometry. It transforms the wall wetted perimeters S_f and the fluid–fluid interface S_i into infinite horizontal parallel (iso) lines defined by (distinct) constant ζ-values for which $-\infty < \xi < +\infty$. We use the definition

$$x = \frac{R \sin \delta_l \sinh \xi}{\cosh \xi + \cos \zeta} \quad \text{and} \quad y = \frac{R \sin \delta_l \sin \zeta}{\cosh \xi + \cos \zeta} \tag{10}$$

which represents a translation $\zeta = \pi - \zeta'$ of the standard definition found in mathematical handbooks and used by most workers. The redefined (ξ, ζ)-axes coincide with the interface and vertical symmetry line of the pipe, respectively. This reference frame has the advantage of yielding symmetric results for the phases g and l with respect to the interface: The interfacial and wall wetted perimeters are now simply given by the isolines $\zeta = 0$ and $\zeta = \pm\delta_f$, respectively, see Fig. 2.

Expressing the particular solutions (8) in the bipolar coordinates (ξ, ζ) as defined by Eq. (10), yields

$$u_f^p = -\frac{B_f R^2 \sin \delta_f \sin(\delta_f \mp \zeta)}{2\eta_f(\cosh \xi + \cos \zeta)} \tag{11}$$

(since $\sin \delta_g = \sin \delta_l$). The boundary value problem for the homogeneous solutions ϕ_f expressed in bipolar coordinates may be obtained by inserting Eq. (7), using Eq. (11), in the boundary value problem (2)–(6). The differential equation (2), yields

$$\frac{\partial^2 \phi_f}{\partial \xi^2} + \frac{\partial^2 \phi_f}{\partial \zeta^2} = 0 \quad \text{in } A_f \tag{12}$$

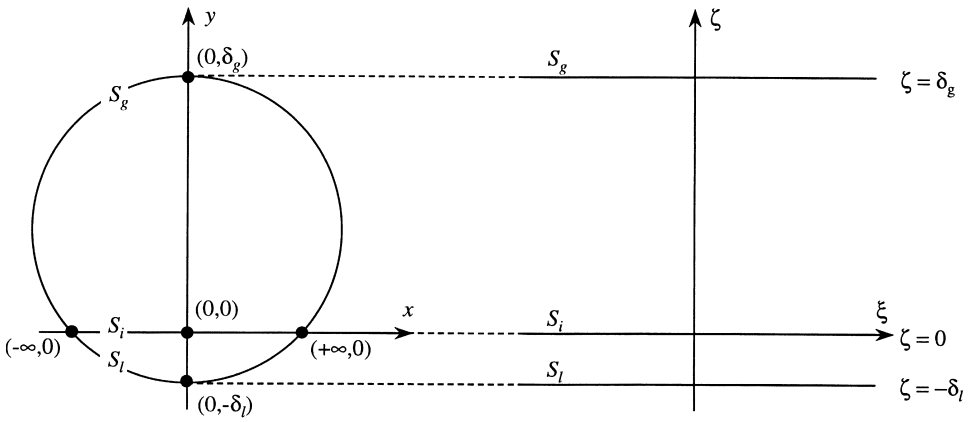

Fig. 2. The pipe cross section in bipolar coordinates.

The no-slip conditions on the pipe walls (4) and interface (5) yield

$$\phi_f(\zeta = \pm\delta_f) = 0 \tag{13}$$

and

$$\phi_l(\zeta = 0) - \phi_g(\zeta = 0) = \frac{R^2}{4}\left(\frac{\eta_g B_l \sin^2 \delta_l - \eta_l B_g \sin^2 \delta_g}{\eta_g \eta_l}\right)\operatorname{sech}^2\left(\frac{\xi}{2}\right) \tag{14}$$

respectively. Finally, the continuous shear stress conditions on the interface (6) yield

$$\eta_f \left.\frac{\partial \phi_f}{\partial \zeta}\right|_{\zeta=0} = \frac{R \sin \delta_f}{2}\left(\tau_i \mp \frac{B_f R \cos \delta_f}{2}\right)\operatorname{sech}^2\left(\frac{\xi}{2}\right) \tag{15}$$

(by use of the chain rule for differentiation and the fact that $\partial\xi/\partial y = 0$ and $\partial\zeta/\partial y = 2\cosh^2(\xi/2)/(R \sin \delta_f)$ for $\zeta = 0$). The boundary value problem for the homogeneous solutions (12)–(15) may now be solved using the Fourier cosine transform pair defined by

$$\tilde{f}(\omega) = \frac{2}{\pi}\int_0^\infty f(\xi) \cos \omega\xi \, \mathrm{d}\xi \tag{16a}$$

$$f(\xi) = \int_0^\infty \tilde{f}(\omega) \cos \omega\xi \, \mathrm{d}\omega \tag{16b}$$

in which $\tilde{f}$ denotes the Fourier cosine transform of f. The Fourier transform (16a) of the differential equations (12) yields

$$\frac{\partial^2 \tilde{\phi}_f}{\partial \zeta^2} - \omega^2 \tilde{\phi}_f = 0 \quad \text{in } \tilde{A}_f \tag{17}$$

The Fourier cosine transform (16a) of the no-slip conditions on the pipe wall and interface (13) and (14) yield

$$\tilde{\phi}_f(\zeta = \pm\delta_f) = 0 \tag{18}$$

and

$$\tilde{\phi}_l(\zeta = 0) - \tilde{\phi}_g(\zeta = 0) = R^2\left(\frac{\eta_g B_l \sin^2 \delta_l - \eta_l B_g \sin^2 \delta_g}{\eta_g \eta_l}\right)\frac{\omega}{\sinh \omega\pi} \tag{19}$$

respectively, after application of the known relation

$$\frac{2}{\pi}\int_0^\infty \operatorname{sech}^2\left(\frac{\xi}{2}\right)\cos \omega\xi \, \mathrm{d}\xi = \frac{4\omega}{\sinh \omega\pi} \tag{20}$$

Finally, applying the Fourier cosine transform (16a) and the relation (20) to the conditions for continuous shear stress at the interface (15) yields

$$\eta_f \frac{\partial \tilde{\phi}_f}{\partial \zeta}|_{\zeta=0} = 2R \sin \delta_f \left(\mathscr{T}_i(\omega) \mp \frac{B_f R \cos \delta_f}{2} \right) \frac{\omega}{\sinh \omega\pi} \tag{21}$$

in which the coefficient $\mathscr{T}_i(\omega)$ is defined by

$$\frac{2}{\pi} \int_0^\infty \tau_i \operatorname{sech}^2\left(\frac{\xi}{2}\right) \cos \omega\xi \, \mathrm{d}\xi = \frac{4\omega}{\sinh \omega\pi} \mathscr{T}_i(\omega) \tag{22}$$

The definition (22) plays a central role in the present analysis. It was introduced in order to keep track of the influence of the interfacial shear stress throughout the equation system. It was chosen by the criterion that $\mathscr{T}_i(\omega) \equiv \tau_i^c = \text{constant}$ in the event that the boundary value problem (2)–(6) is simplified to that of a single fluid f subject to a *constant* (prescribed) surface shear stress distribution $\tau_i \equiv \tau_i^c = \text{constant}$, as studied in Biberg (1999b). Whether this criterion is satisfied may be realized by comparing Eq. (22) with (20). The definition (22) does thus have the interesting side effect of reducing the equations given here to the corresponding expressions for a single fluid f subject to a *constant* surface shear stress by simply replacing any occurrence of $\mathscr{T}_i(\omega)$ with $\tau_i^c = \text{constant}$. (This does *not*, however, apply to the results of the triple point analysis given in Appendix B, as will be explained later.)

Considering the no-slip conditions on the pipe wall (18), the solutions of Eq. (17) may be written

$$\tilde{\phi}_f = C_f(\omega) \sinh\big(\omega\big(\delta_f \mp \zeta\big)\big) \tag{23}$$

in which the coefficients $C_f(\omega)$ are determined by the continuous shear stress conditions (21), yielding

$$C_f(\omega) = \frac{2R \sin \delta_f}{\eta_f} \left(\frac{B_f R \cos \delta_f}{2} \mp \mathscr{T}_i(\omega) \right) \frac{1}{\sinh \omega\pi \cosh \omega\delta_f} \tag{24}$$

The coefficient $\mathscr{T}_i(\omega)$ is now given by use of the no-slip condition on the interface (19), yielding

$$\mathscr{T}_i(\omega) = \frac{R\left\{\eta_g B_l\left[\sin \delta_l - \left(\frac{\tanh \omega\delta_l}{\omega}\right)\cos \delta_l\right] - \eta_l B_g\left[\sin \delta_g - \left(\frac{\tanh \omega\delta_g}{\omega}\right)\cos \delta_g\right]\right\}}{2\left[\eta_g\left(\frac{\tanh \omega\delta_l}{\omega}\right) + \eta_l\left(\frac{\tanh \omega\delta_g}{\omega}\right)\right]} \tag{25}$$

Now as $\mathscr{T}_i(\omega)$ is known, Eq. (22) determines the interfacial shear stress distribution i.e. applying the inverse Fourier cosine transform (16b) to Eq. (22), yields

$$\tau_i = 4 \cosh^2\left(\frac{\xi}{2}\right) \int_0^\infty \mathscr{T}_i(\omega) \frac{\omega \cos \omega\xi}{\sinh \omega\pi} \, \mathrm{d}\omega \quad \text{for} \quad -\infty \le \xi \le \infty \tag{26}$$

The definition (22) thus causes the expression for the interfacial shear stress distribution (26) to be determined by the no-slip condition on the interface (5) as part of the solution for velocity field, in complete analogy with the corresponding channel flow problem, see Eq. (A5) in Appendix A. Applying the inverse Fourier transform (16b) to Eq. (23) yields the homogeneous

solutions ϕ_f. Eq. (7) may thus be written as

$$u_f = u_f^p + \int_0^\infty C_f(\omega)\sinh\big(\omega\big(\delta_f \mp \zeta\big)\big)\cos\,\omega\xi\,\mathrm{d}\omega \tag{27}$$

Inserting Eqs. (11) and (24) in Eq. (27) yields the final solution for the velocity field, given by

$$\begin{aligned} u_f = &\overbrace{-\frac{B_f R^2 \sin\delta_f}{2\eta_f}\left[\frac{\sin\big(\delta_f \mp \zeta\big)}{\cosh\,\xi + \cos\,\zeta} - 2\cos\,\delta_f \int_0^\infty \frac{\sinh\big(\omega\big(\delta_f \mp \zeta\big)\big)}{\sinh\,\omega\pi\,\cosh\,\omega\delta_f}\cos\,\omega\xi\,\mathrm{d}\omega\right]}^{\text{free surface flow}} \\ &\overbrace{\mp\frac{2R\sin\delta_f}{\eta_f}\int_0^\infty \mathscr{T}_i(\omega)\frac{\sinh\big(\omega\big(\delta_f \mp \zeta\big)\big)}{\sinh\,\omega\pi\,\cosh\,\omega\delta_f}\cos\,\omega\xi\,\mathrm{d}\omega}^{\text{shear flow}} \quad \text{for}\begin{cases} -\infty \le \xi \le \infty \\ \delta_f \le \pm\zeta \le 0 \end{cases} \end{aligned} \tag{28}$$

Eq. (28) is a generic expression for the velocity field in phase f for a given pressure drop and holdup, represented by the driving forces $-B_f$ and wetted angles δ_f, respectively, see Eqs. (3) and (9). The expression may be demonstrated to be equivalent to the separate expressions for the phases $f = g$ or l obtained by Semenov and Tochigin (1961) using the more inconvenient (asymmetrical) ξ and $\zeta' = \pi - \zeta$ coordinate system. The introduction of the coefficient $\mathscr{T}_i(\omega)$ given by Eq. (25) has given us the additional advantage of splitting the solution (28) into a linear combination of two terms with distinct physical interpretations. The key to interpreting these terms is given by the fact that $\mathscr{T}_i(\omega)$ represents the influence of the interfacial shear stress, through the definition (22). The interfacial shear stress does thus not affect the first term in Eq. (28). In fact, the velocity field (28) reduces to this term for $\tau_i = 0$, for which $\mathscr{T}_i(\omega) \equiv 0$ by Eq. (22), and the second (shear flow) term vanishes. The first term in Eq. (28) therefore represents the single-phase free surface flow of fluid f due to a given body force $-B_f$. The shear flow term in Eq. (28) acts as a coupling term between the phases and represents the part of the velocity field in phase f given by the interfacial drag from the opposite phase.

It may be useful to compare the velocity field (28) with the corresponding, however, significantly more transparent expression in channel flow, see Eq. (A4) in Appendix A. It may also be interesting to note that $\mathscr{T}_i(\omega)$ reduces to the *constant* interfacial shear stress distribution in the special case of equal fluid properties i.e.

$$\mathscr{T}_i(\omega) = \pm\frac{B_f R\cos\delta_f}{2} \quad \text{for}\begin{cases} \rho_g = \rho_l \\ \eta_g = \eta_l \end{cases} \tag{29}$$

This relation may be used to check the single-phase limit in the equations: Introducing Eq. (29) in (24) yields $C_f(\omega) = 0$. The velocity fields (27) thus reduce to the Hagen–Poiseuille solutions for single-phase flow (8). Moreover, introducing Eq. (29) in the expression for the interfacial shear stress distribution (26) yields

$$\tau_i = \pm\frac{B_f R\cos\delta_f}{2}\overbrace{\left[4\cosh^2\left(\frac{\xi}{2}\right)\int_0^\infty \frac{\omega\cos\omega\xi}{\sinh\omega\pi}\,\mathrm{d}\omega\right]}^{=1} = \pm\frac{B_f R\cos\delta_f}{2} \quad \text{for} \begin{cases}\rho_g=\rho_l\\ \eta_g=\eta_l\end{cases} \tag{30}$$

further proving consistency. (The expression in the square brackets may be evaluated to unity by application of the inverse Fourier cosine transform (16b) of Eq. (20).)

4. Wall and interfacial shear stress distributions

The shear stress distribution may be obtained by a formal differentiation of the velocity field (28). We are mainly interested in the wall and interfacial shear stresses. Both the pipe wall and the fluid–fluid interface are described by surfaces where $\zeta =$ constant, see Fig. 2. The shear stress in the z-direction (direction of flow) on a surface $\zeta =$ constant, is given by

$$\tau_{f,\zeta,z} = \eta_f\left(\frac{\cosh\xi+\cos\zeta}{R\sin\delta_f}\right)\frac{\partial u_f}{\partial\zeta} \tag{31}$$

The wall shear stresses τ_f, defined in Fig. 1, are thus given by

$$\tau_f = \mp\tau_{f,\zeta,z}\big(\zeta=\pm\delta_f\big) \tag{32}$$

Formally, carrying out the differentiation implied by Eq. (31), using Eq. (28) and considering Eq. (32), thus yields the final expression for the wall shear stresses, given by

$$\begin{aligned}\tau_f = &\overbrace{-\frac{B_f R}{2}\left[1-2\big(\cosh\xi+\cos\delta_f\big)\cos\delta_f\int_0^\infty\frac{\omega\cos\omega\xi}{\sinh\omega\pi\cosh\omega\delta_f}\,\mathrm{d}\omega\right]}^{\text{free surface flow}}\\ &\overbrace{\mp 2\big(\cosh\xi+\cos\delta_f\big)\int_0^\infty\mathscr{T}_i(\omega)\frac{\omega\cos\omega\xi}{\sinh\omega\pi\cosh\omega\delta_f}\,\mathrm{d}\omega}^{\text{shear flow}} \quad \text{for } -\infty\le\xi\le\infty\end{aligned} \tag{33}$$

in which the contributions from the free-surface-flow and shear flow terms in Eq. (28) are indicated. The first term in Eq. (33) thus equals the shear stress in free surface flow due to a given body force $-B_f$, whereas the second term represents the shear stress given by the interfacial drag from the opposite phase. Applying Eq. (29), we find that Eq. (33) yields the correct constant shear stress $\tau_f = -B_f R/2$ in the single-phase case of equal fluid properties.

The expression for the interfacial shear stress distribution (26) was obtained as part of the solution for the velocity field (28). As a consistency check, however, the identical expression may be obtained by differentiation using Eq. (31) with $\zeta = 0$, and either of the velocity fields $f = g$ or l as given by Eq. (28). The contribution from the free surface, flow term in the velocity field may be demonstrated to be zero (in agreement with the definition), whereas the

contribution from the shear flow term yields Eq. (26). The expression for the shear stress on the vertical symmetry line of the pipe $\xi = 0$, used in some of the numerical examples to follow, may be obtained by using Eqs. (28) and (31) and will not be given here. The shear stress distributions (33) and (26) agree with the corresponding expressions for horizontal flow, derived from Bentwich's (1964) circular interface (and horizontal flow) solution by Brauner et al. (1996a). The expressions (33) and (26), however, include the effect of a pipe inclination.

5. Wall and interfacial shear stress in the triple points

An interesting aspect of the wall and interfacial shear stresses (33) and (26) is their limiting behaviour in the triple points $\xi \to \pm\infty$, where the fluid–fluid interface meets the pipe wall, see Fig. 2. Due to symmetry it suffices to consider e.g. $\xi \to \infty$. The correct limiting behaviour may then be obtained by use of residue calculus. A complete analysis, yielding the results presented in this section, is given in Appendix B. We start by noting that the equal viscosity case $\eta_g/\eta_l = 1$ must be treated separately. This is also the situation for the high and low viscosity ratio limits $\eta_g/\eta_l \to \infty$ and $\eta_g/\eta_l \to 0$, respectively, in the event that the more viscous fluid occupies a larger portion of the pipe cross section. Otherwise, these limits are contained in the remaining analysis, which for $\eta_g/\eta_l < 1$ is divided into the three distinct cases: $\delta_l < \pi/2$, $\delta_l = \pi/2$ and $\delta_l > \pi/2$. Two-phase symmetry assures that the corresponding cases for $\eta_g/\eta_l > 1$ are given by simply switching the indices g and l in the analysis yielding the results for $\eta_l/\eta_g < 1$ and $\delta_g < \pi/2$, $\delta_g = \pi/2$ or $\delta_g > \pi/2$ (i.e. $\eta_g/\eta_l > 1$ and $\delta_l > \pi/2$, $\delta_l = \pi/2$ or $\delta_l < \pi/2$, respectively). Two-phase symmetry also provides the results for the high viscosity ratio limit $\eta_g/\eta_l \to \infty$ i.e. $\eta_l/\eta_g \to 0$ from the low viscosity ratio limit $\eta_g/\eta_l \to 0$. When utilizing two-phase symmetry, however, the opposite sign in the interfacial shear stress as seen by the fluids g and l must be a accounted for.

Generally, the wall and interfacial shear stresses will all be zero in the triple points if the more viscous fluid occupies a smaller portion of the pipe cross section. We thus have

$$\tau_f(\xi \to \infty) = \tau_i(\xi \to \infty) = 0 \quad \text{for} \begin{cases} \delta_l < \pi 2 \\ \eta_g/\eta_l < 1 \end{cases} \tag{34}$$

The interfacial shear stress remains zero in the triple points when the fluids occupy exactly half the pipe cross section each. The wall shear stresses, however, attain finite and generally non-zero limits. We have

$$\tau_f(\xi \to \infty) = -\frac{B_f R}{2} \mp \frac{(\eta_g B_l - \eta_l B_g)R}{2(\eta_g + \eta_l)} \quad \text{and} \quad \tau_i(\xi \to \infty) = 0 \quad \text{for} \begin{cases} \delta_l = \pi/2 \\ \eta_g/\eta_l < 1 \end{cases} \tag{35}$$

There is thus in this case a discontinuity in the wall shear stress across the interface, given by

$$\tau_l(\xi \to \infty) - \tau_g(\xi \to \infty) = -\frac{R}{2}(B_g + B_l)\left(\frac{\eta_l - \eta_g}{\eta_g + \eta_l}\right) \quad \text{for} \begin{cases} \delta_l = \pi/2 \\ \eta_g/\eta_l < 1 \end{cases} \tag{36}$$

We also note that Eq. (35) yields $\tau_g(\xi\to\infty)=\tau_i(\xi\to\infty)=0$, whereas $\tau_l(\xi\to\infty)=-R(B_g+B_l)/2$ for $\eta_g/\eta_l\to 0$.

If the more viscous fluid occupies a larger portion of the pipe cross section and $\eta_g/\eta_l\neq 0$ or ∞, the wall and interfacial shear stresses tend to infinity. The limiting behaviours are given by

$$\tau_f(\xi\to\infty)\sim\frac{K\mathrm{e}^{(1-v_0)\xi}}{|\cos\delta_f v_0|}\quad\text{and}\quad\tau_i(\xi\to\infty)\sim-K\mathrm{e}^{(1-v_0)\xi}\quad\text{for}\begin{cases}\delta_l>\pi/2\\0<\eta_g/\eta_l<1\end{cases}\tag{37}$$

in which K and $0<v_0<1$ are given by Eqs. (B11) and (B7) in Appendix B. The sign of the wall shear stresses in the vicinity of the triple point are thus equal and opposite to that of the interfacial shear stress. (In e.g. horizontal flow $K>0$ for $\eta_g/\eta_l<1$. In this case, the wall shear stresses thus tend to infinity through positive values when approaching the triple point, whereas the interfacial shear stress becomes negative.) The wall and interfacial shear stresses remain integrable, even though the triple point limits tend to infinity. This may be confirmed by multiplying triple point limits (37) with the appropriate differential elements along the pipe wall or interface, given by

$$\mathrm{d}S=\frac{R\sin\delta_f\,\mathrm{d}\xi}{\cosh\xi+\cos\zeta}\tag{38}$$

with $\zeta=\pm\delta_f$ or $\zeta=0$, respectively. The fact that the corresponding $\mathrm{d}S\sim 2R\sin\delta_f\mathrm{e}^{-\xi}\,\mathrm{d}\xi$ for $\xi\to\infty$ proves the integrability.

We now turn to the special cases. We start with considering the low viscosity ratio limit $\eta_g/\eta_l\to 0$. The corresponding triple point limits are contained in the above analysis provided that the more viscous fluid l occupies up to half the pipe cross section. The special case in which fluid l occupies more than half the pipe cross section, however, yields

$$\tau_g(\xi\to\infty)=\tau_i(\xi\to\infty)=0\quad\text{and}\quad\tau_l(\xi\to\infty)\sim\frac{\pi^2}{\delta_l^2\sin\frac{\pi^2}{2\delta_l}}\mathrm{e}^{-\frac{\pi}{2\delta_l}\xi}\quad\text{for}\begin{cases}\delta_l>\pi/2\\\eta_g/\eta_l\to 0\end{cases}\tag{39}$$

The results (34), (35) and (39), combined with two-phase symmetry, show that the shear stress as seen by the less viscous fluid is zero in the triple points in the high and low viscosity ratio limits $\eta_g/\eta_l\to\infty$ and $\eta_g/\eta_l\to 0$, irrespective of holdup. The corresponding wall shear stress in the more viscous fluid, however, is generally zero in the triple points if the more viscous fluid occupies less than half the pipe cross section. It attains a finite, generally non-zero, triple point limit if the more viscous fluid occupies exactly half the pipe cross section, and tends to infinity if the more viscous fluid occupies more than half the pipe cross section.

In the final special case of equal fluid viscosities i.e. $\eta_g/\eta_l=1$, the wall and interfacial shear stresses attain the following finite limits in the triple points irrespective of holdup

$$\tau_f(\xi\to\infty)=-\frac{R}{2}\left(B_g\epsilon_g+B_l\epsilon_l\right)\quad\text{and}\quad\tau_i(\xi\to\infty)=\pm\frac{R\cos\delta_f}{2}\left(B_g\epsilon_g+B_l\epsilon_l\right)\quad\text{for}\quad\eta_g/\eta_l=1\tag{40}$$

The wall shear stresses are thus in this case continuous across the interface. We also have that

$\tau_f(\xi\to\infty) = \pm\tau_i(\xi\to\infty)/\cos\delta_f$. Moreover, there are no two-phase effects in horizontal flow, since horizontal flow implies that $B_l/B_g = 1$, which combined with equal viscosities causes the fluids to behave as one (we will return to this point in Section 7.1). In horizontal flow, the triple point limits (40) thus reduce to the single-phase values $\tau_f = -B_f R/2$ and $\tau_i = \pm B_f R\cos\delta_f/2$, respectively (considering that $\epsilon_g + \epsilon_l = 1$). As a consistency check, we note that $B_l/B_g \equiv 1$ for equal fluid densities, i.e. $\rho_g/\rho_l = 1$ irrespective of pipe inclination. In the single-phase case of equal viscosities and densities, the triple point limits (40) thus reduce identically to the correct single-phase value.

6. Mean wall and interfacial shear stress

The mean wall and interfacial shear stresses are given by integration of the corresponding shear stress distributions (33) and (26), respectively. Formally we have

$$\bar{\tau}_f = \frac{1}{S_f}\int_{S_f}\tau_f\,\mathrm{d}S \tag{41a}$$

and

$$\bar{\tau}_i = \frac{1}{S_i}\int_{S_i}\tau_i\,\mathrm{d}S \tag{41b}$$

in which the overbar indicates mean values, and the wall and interfacial perimeters are given by

$$S_f = D\delta_f \tag{42a}$$

and

$$S_i = D\sin\delta_f \tag{42b}$$

respectively, where $D = 2R$. The expression for the mean interfacial shear stress may be obtained from (41b) using (42b), (26) and (38) with $\zeta = 0$, yielding

$$\bar{\tau}_i = \frac{2}{\pi}\int_0^\infty\int_0^\infty\left[\mathscr{T}_i(\omega)\frac{\omega\pi}{\sinh\omega\pi}\right]\cos\omega\xi\,\mathrm{d}\omega\,\mathrm{d}\xi \tag{43}$$

We now utilize the fact that Fourier cosine transform (16a) of the inverse Fourier cosine transform (16b) at $\omega = 0$, yields

$$\frac{2}{\pi}\int_0^\infty\int_0^\infty\tilde{f}(\omega)\cos\omega\xi\,\mathrm{d}\omega\,\mathrm{d}\xi = \lim_{\omega\to 0^+}\tilde{f}(\omega) \tag{44}$$

Applying this relation to Eq. (43) yields

$$\bar{\tau}_i = \lim_{\omega\to 0}\mathscr{T}_i(\omega) \tag{45}$$

since

$$\lim_{\omega\to 0}\frac{\omega\pi}{\sinh\omega\pi}=1 \tag{46}$$

Finally, taking the limit in Eq. (45) using (25) and the fact that $\tanh(\omega\delta)/\omega=\delta$ for $\omega\to 0$, we obtain the following remarkably simple and exact expression for the mean interfacial shear stress, given by

$$\bar{\tau}_i=\frac{R\left[\eta_g B_l(\sin\delta_l-\delta_l\cos\delta_l)-\eta_l B_g\left(\sin\delta_g-\delta_g\cos\delta_g\right)\right]}{2\left(\eta_g\delta_l+\eta_l\delta_g\right)} \tag{47}$$

Introducing Eq. (3) in (47) and rearranging slightly, yields the alternative form, given by

$$\bar{\tau}_i=\frac{\pi R}{2\left(\eta_g\delta_l+\eta_l\delta_g\right)}\left[\eta_g\left(\frac{\partial p}{\partial z}+\rho_l g\sin\theta\right)F(\delta_l)-\eta_l\left(\frac{\partial p}{\partial z}+\rho_g g\sin\theta\right)F\left(\delta_g\right)\right] \tag{48}$$

where

$$F\left(\delta_f\right)=\frac{1}{\pi}\left(\sin\delta_f-\delta_f\cos\delta_f\right)$$

Eq. (48) is regarded to be one of the main results of the present analysis, and will be discussed in some more detail in Section 7. It may, however, be noted that Eq. (48) attains the correct single-phase limit in case of equal fluid properties, as given by the right-hand side of Eq. (29). It is also interesting to observe the similarity between Eqs. (47) and (48) and the corresponding expressions in channel flow, as given by Eqs. (A5) and (A6) in Appendix A.

The expressions for the mean wall shear stresses may be found by inserting the expressions for the wall shear stresses distribution (33) in (41a). It is more convenient, however, to apply Eqs. (31) and (32) to Eq. (27). Using the resulting expression in Eq. (41a) immediately yields

$$\bar{\tau}_f=-\frac{B_f R}{2}+\frac{\eta_f}{S_f}\frac{2}{\pi}\int_0^\infty\int_0^\infty\left[C_f(\omega)\omega\pi\right]\cos\omega\xi\,\mathrm{d}\omega\,\mathrm{d}\xi \tag{49}$$

The first term in Eq. (49) is the contribution from the (Hagen–Poiseuille) particular solution (8), and thus equals the wall shear stress in single-phase flow of fluid f. The second term in Eq. (49) may be developed further by application of Eq. (44). Eq. (24) combined with Eqs. (45) and (46), yields

$$\lim_{\omega\to 0}C_f(\omega)\omega\pi=\frac{2R\sin\delta_f}{\eta_f}\left(\frac{B_f R\cos\delta_f}{2}\mp\bar{\tau}_i\right) \tag{50}$$

Applying Eq. (44) to (49) using Eqs. (42) and (50), thus yields

$$\bar{\tau}_f=-\frac{B_f}{S_f}\left(\delta_f-\frac{1}{2}\sin 2\delta_f\right)R^2\mp\frac{S_i}{S_f}\bar{\tau}_i \tag{51}$$

Now, noting that $\epsilon_f\pi R^2=A_f$ or that

$$\left(\delta_f - \frac{1}{2}\sin 2\delta_f\right)R^2 = A_f \tag{52}$$

by Eq. (9), yields the final result for the mean wall shear stresses, given by

$$\bar{\tau}_f = -B_f\frac{A_f}{S_f} \mp \frac{S_i}{S_f}\bar{\tau}_i \tag{53}$$

Introducing Eq. (3) in (53) and rearranging, however, we have

$$A_f\left(\frac{\partial p}{\partial z} + \rho_f g \sin\theta\right) + \bar{\tau}_f S_f \pm \bar{\tau}_i S_i = 0 \tag{54}$$

which is recognized as the momentum balance for fluid f. We have thus recaptured the momentum balances from the solution for the velocity field. The momentum balances may be obtained by direct integration of the differential equations (2), or even more conveniently by simply equating the forces acting on the fluids to zero. Arriving at the momentum balances starting with the laminar flow solution, as demonstrated here, however, confirms the consistency of the equations. It is interesting to study the analogous development in channel flow, see Eqs. (A7)–(A9).

7. Discussion

We start the discussion by noting that it may be helpful to study the analogous, however, mathematically significantly more transparent channel flow problem, solved in Appendix A, in order to fully understand the equations developed in the previous sections. The two-phase stratified flow geometry in a pipe, defined in Fig. 1, tends to complicate the pipe flow solution. We have, however, simplified the equations by placing the (bipolar) coordinate axes on the interface and vertical symmetry line of the pipe respectively, see Fig. 2. This is the appropriate reference frame for the flow. It emphasizes two-phase symmetry, yielding the distinct advantage that corresponding expressions for the phases g and l may be written into a single generic expression for the general phase f as in the solution for the velocity field (28). A further simplification is given by the introduction of the coefficient $\mathscr{T}_i(\omega)$ representing the interfacial shear stress distribution through the definition (22). The coefficient $\mathscr{T}_i(\omega)$ allows us to split the solution (28) into a single-phase free surface flow term and a two-phase shear flow coupling term representing the Poiseuille and Couette flow parts of the solution, respectively. The definition of the $\mathscr{T}_i(\omega)$ has the additional advantage that the expression for the interfacial shear stress distribution (26) emerges naturally as a consequence of the no-slip condition at the interface, in complete analogy with the situation in channel flow. The definition (22) of $\mathscr{T}_i(\omega)$ was chosen by the criterion that the solution for each phase (28) should reduce identically to the solution for a single fluid f subject to a *constant* (prescribed) interfacial shear stress distribution $\tau_i^c = \text{constant}$ if $\mathscr{T}_i(\omega)$ is replaced by τ_i^c. The corresponding velocity and wall shear stress distributions are thus given by introducing $\mathscr{T}_i(\omega) \equiv \tau_i^c = \text{constant}$ in Eqs. (28) and (33), respectively. Moreover, inserting $\mathscr{T}_i(\omega) \equiv \tau_i^c = \text{constant}$ in the expression for the interfacial

shear stress (26) yields the consistent result $\tau_i \equiv \tau_i^c$, by the same token as in Eq. (30). The constant interfacial shear stress case[2] has been considered in Biberg (1999b).

One of the main results given here, is the remarkably simple exact expression for the mean interfacial shear stress (48) in terms of holdup (through δ_f) and pressure drop. (Note that: the wetted angles δ_f are uniquely determined by a given holdup ϵ_l through Eq. (9) and the fact that $\epsilon_g = 1 - \epsilon_l$.) The fluid momentum balances (54) may be viewed as a set of two equations for the three unknown mean wall and interfacial shear stresses, for a given holdup and pressure drop in a given pipe containing a given pair of fluids. The momentum balances of course, simply represent the result of equating the mean forces acting on the fluids to zero. The new expression for the mean interfacial shear stress (48), however, represents the local solution of the boundary value problem (2)–(6) at the interface, i.e. information not obtainable from a regular mean force balance. This expression thus closes the problem, allowing for the computation of the exact general solution for the mean wall and interfacial shear stresses for a given holdup and pressure drop. This may be realized when solving the momentum balances (54) for the wall shear stresses yielding Eq. (53), which should then be combined with Eqs. (3), (9), (42), (48) and the fact that $A_f = \epsilon_f \pi R^2$. The interrelation between the momentum balances (54) and the interfacial shear stress (48) may become clarified by studying the corresponding expressions in channel flow, Eqs. (A9) and (A6) in Appendix A, respectively.

7.1. The scaled equations

The mean velocity and wall shear stress in single-phase flow of fluid g are given by

$$U_g^s = -\frac{B_g R^2}{8\mu_g} \tag{55a}$$

and

$$\tau_g^s = -\frac{B_g R}{2} \tag{55b}$$

respectively. Scaling the mean wall and interfacial shear stresses (53) and (48) by (55b) yields the dimensionless wall and interfacial shear stresses, given by

$$\frac{\bar{\tau}_g}{\tau_g^s} = \left(\frac{\delta_g - \frac{1}{2}\sin 2\delta_g}{\delta_g}\right) - \frac{\sin\delta_g}{\delta_g}\frac{\bar{\tau}_i}{\tau_g^s} \tag{56}$$

$$\frac{\bar{\tau}_l}{\tau_g^s} = \frac{B_l}{B_g}\left(\frac{\delta_l - \frac{1}{2}\sin 2\delta_l}{\delta_l}\right) + \frac{\sin\delta_l}{\delta_l}\frac{\bar{\tau}_i}{\tau_g^s} \tag{57}$$

[2] It may be noted that a constant interfacial shear stress distribution implies that $\tau_i \equiv \tau_i^c$ in the triple points (irrespective of holdup). The corresponding limiting behaviour of the wall shear stress is given by $\tau_f(\xi \to \pm\infty) = \pm\tau_i^c/\cos\delta_f$ for $\delta_f < \pi/2$ and $\tau_f(\xi \to \pm\infty) = \infty$ for $\delta_f \geq \pi/2$, see Biberg (1999b). These limits differ from the laminar–laminar flow values, derived in Section 5.

$$\frac{\bar{\tau}_i}{\tau_g^s} = \frac{\pi}{\delta_g + (\eta_g/\eta_l)\delta_l}\left[F(\delta_g) - \frac{\eta_g}{\eta_l}\frac{B_l}{B_g}F(\delta_l)\right] \tag{58}$$

in which we have used Eqs. (9) and (42) and the fact that $A_f = \epsilon_f \pi R^2$ in order to display the holdup dependency through δ_f. We note that the dimensionless mean shear stresses (56)–(58) are completely determined by the viscosity and driving force ratios η_g/η_l and B_l/B_g, respectively, for a given holdup i.e. δ_f. This is also the case for the corresponding dimensionless velocity field, as given by scaling (28) with (55a). We will now (at least to some extent) attempt to analyse the effect of these parameters one at a time.

7.2. Horizontal or friction dominated flow

The driving forces in the direction of flow B_f are defined by Eq. (3). In a horizontal pipe the driving force ratio B_g/B_l is equal to unity since the pressure gradient $\partial p/\partial z$ is equal in both phases and the body forces in the direction of flow $\rho_f g \sin\theta$ are zero. The non dimensionalized laminar flow (defined in the previous section) is thus in this case completely determined by the viscosity ratio η_g/η_l for a given holdup. The flow in an inclined pipe will closely resemble the flow in a horizontal pipe provided the pressure gradient is sufficiently large with respect to the body forces in the more dense fluid l — i.e. when $|\rho_l g \sin\theta/(\partial p/\partial z)| \ll 1$ yielding $B_g/B_l \approx 1$. The pressure gradient is in this case balanced by the wall shear stresses, and the flow may be characterized as *friction dominated*. Fig. 3 shows a complete picture of the possible values for the non-dimensional mean wall and interfacial shear stresses (56)–(58), in the horizontal or friction dominated flow.The mean interfacial shear stress (right hand plot) is seen to increase as the viscosity ratio decreases. It is higher than in single-phase flow for which $\eta_g/\eta_l = 1$, when $\eta_g/\eta_l < 1$ and lower when $\eta_g/\eta_l > 1$. The increase in the interfacial shear stress for a decrease in the viscosity ratio is caused by the corresponding increase in the velocity in fluid g, with respect to the velocity in fluid l. Generally, the interfacial shear stress is positive below a certain threshold holdup lying above or below $\delta_f = \pi/2$, depending on whether $\eta_g/\eta_l < 1$ or > 1, respectively. For a given pressure gradient there are thus always holdup values for which fluid g is pulling fluid l and vice versa. The interfacial shear stress is, however,

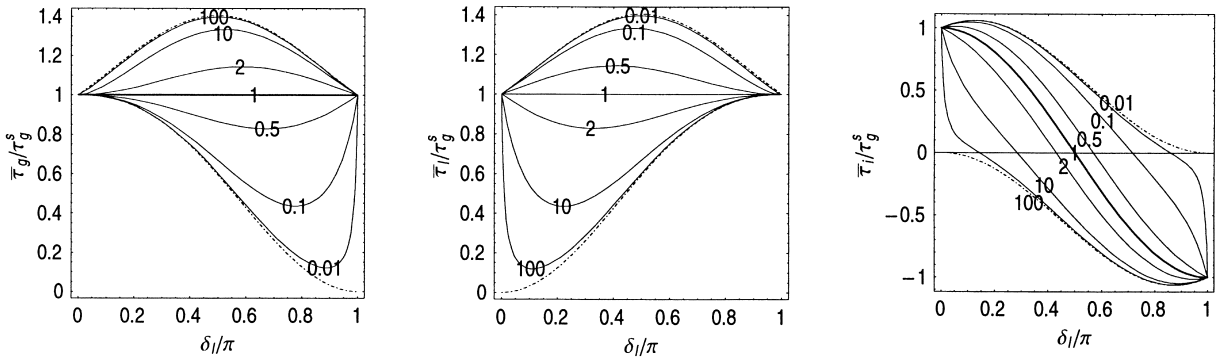

Fig. 3. Dimensionless mean wall and interfacial shear stress as given by Eqs. (56) and (58) in horiziontal and friction dominated flow for $\eta_g/\eta_l = 0.01, \ldots, 100$. The limits $\eta_g/\eta_l \to 0$ are indicated by the dash-dot lines.

seen to be either positive or negative — irrespective of holdup — in the limiting cases where $\eta_g/\eta_l \to 0$ or $\eta_g/\eta_l \to \infty$, respectively (dash-dot lines). These cases correspond to a physical situation in which the more viscous fluid "freezes" with respect to the less viscous fluid, which in this case flows on as in single-phase closed duct flow.

The symmetry in the mean wall shear stress (56)–(57), in horizontal or friction dominated flow ($B_g/B_l = 1$) may be observed in the left hand and center plots in Fig. 3. (The plots would be identical if $\bar{\tau}_g/\tau_g^s$ were plotted vs. δ_g/π). The mean wall shear stress in the more viscous fluid is higher than in single-phase flow (unity), whereas the mean wall shear stress in the less viscous fluid is lower. This is caused by the fact that the more viscous fluid represents a slower flow from the viewpoint of the less viscous fluid. The associated increased drag, opposing the direction of flow, thus causes the corresponding velocity and wall shear stress to decrease. From the viewpoint of the more viscous fluid, however, the presence of the less viscous fluid represents a faster flow. The associated increased drag, in the direction of flow, causes the corresponding velocity and wall shear stress to increase. The highest possible mean wall shear stress in horizontal or friction dominated flow: $\bar{\tau}_f/\tau_g^s = 1 + 4/\pi^2 \approx 1.41$ is obtained for $\delta_f = \pi/2$ in fluid g or l as $\eta_g/\eta_l \to \infty$ or $\eta_g/\eta_l \to 0$, respectively.

Fig. 4 shows the wall and interfacial shear stress distributions (33) and (26) corresponding to the mean values in Fig. 3 for $\eta_g/\eta_l = 1$, 0.5, 0.1, 0.01, 0 and $\delta_l = \pi/4$, $\pi/2$, $3\pi/4$. The velocity and shear stress distributions on the vertical symmetry line of the pipe as given by (28) and (31) for $\xi = 0$ are also shown. They are plotted as functions of the dimensionless distance $(y + h)/D$ from the bottom of the pipe, where h is the depth of fluid l. The wall shear stress is plotted as a function of pipe inner perimeter measured in degrees from the bottom of the pipe. The interfacial shear stress is plotted on half the interface from the vertical symmetry line to the pipe wall, in terms of the dimensionless coordinate $x/R \sin \delta_l$. The velocity and shear stress distributions in Fig. 4 are non dimensionalized using (55a) and (55b), respectively.

The shear stress distributions in Fig. 4 are consistent with the corresponding mean values in Fig. 3. Moreover, the limiting behaviour in the triple points at the interface agrees with the analysis in Section 5. We note in particular that the interfacial shear stress and the wall shear stress in the less viscous fluid g are zero in the triple points in the zero viscosity ratio limit $\eta_g/\eta_l \to 0$, irrespective of holdup (see dash dot lines). The triple point limits agree with the single-phase closed duct flow situation experienced by fluid g in this case. It is also interesting to observe the increasingly nonlinear behaviour of the shear stress on the vertical symmetry line as the viscosity ratio decreases. The corresponding shear stress in horizontal or friction dominated channel flow is by comparison given as a single straight line across the entire channel irrespective of viscosity ratio, see Eq. (A7) in Appendix A with $B_g/B_l = 1$. Another interesting detail may be observed when studying the velocity and shear stress profiles for $\delta_l = 3\pi/4$ and $\eta_g/\eta_l = 0.1$ (marked $\otimes$) in Fig. 4. The velocity profile is in this case seen to be near vertical across the interface and the interfacial shear stress low. Both fluids are thus close to being in free surface flow in this case. This is confirmed by the corresponding low value of mean interfacial shear stress in Fig. 3. For the higher viscosity ratio $\eta_g/\eta_l = 0.5$, the mean interfacial shear stress is negative and fluid l is pulling fluid g, see Fig. 3. The opposite is the case for the lower viscosity ratio $\eta_g/\eta_l = 0.01$.

Two-phase symmetry facilitates the study of the horizontal or friction dominated flow case in which the upper less dense fluid g is the more viscous and $\eta_g/\eta_l = 1$, 2, 10, 100, ∞, by simply

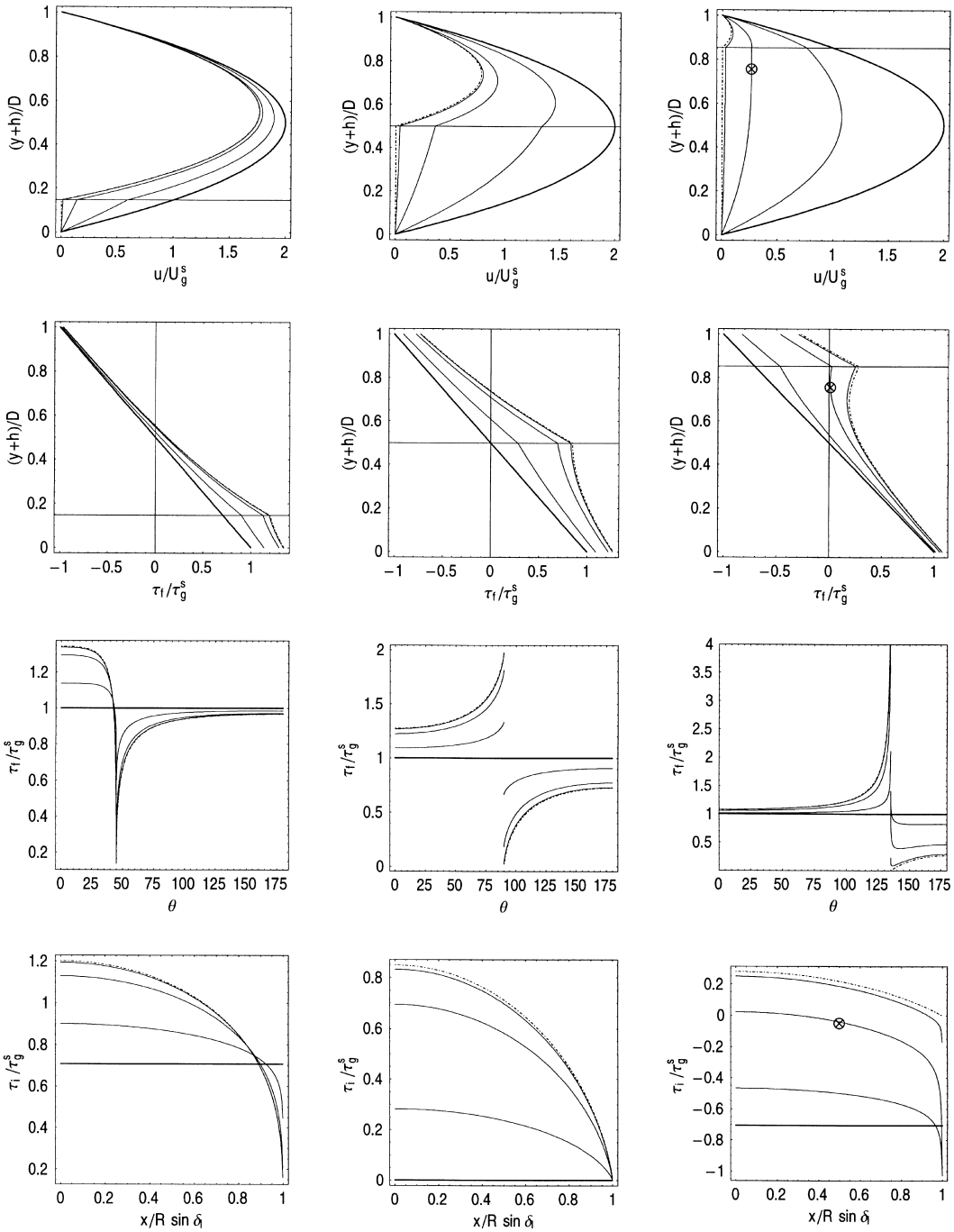

Fig. 4. Velocity and shear stress distributions in horizontal or friction dominated flow. Top two rows: velocity and shear stress on vertical symmetry line. Bottom rows: wall and interfacial shear stress. Columns left to right: $\delta_l = \pi/4, \pi/2, 3\pi/4$. Thick solid lines: single-phase flow $\eta_g/\eta_l = 1$. Thin solid lines: two-phase flow with $\eta_g/\eta_l = 0.5, 0.1, 0.01$. Dash dot lines: limit $\eta_g/\eta_l \to 0$.

turning Fig. 4 upside down. The sign of the interfacial shear stress and the shear stress on the vertical symmetry line must, however, in this case be reversed, if the positive directions as defined in Fig. 1 are to be kept. It must also be understood that; the positive flow direction is now from right to left; the velocity is scaled by the mean velocity for single-phase flow of fluid l i.e. $U_l^s = -B_l R^2/8\mu_l$; the dash-dot line indicates the limit $\eta_g/\eta_l = \infty$; the distance $(y + h)/D$ is measured from the top of the pipe (h = depth of fluid g); and finally that the wall shear stress is plotted as a function of pipe inner perimeter measured in degrees from the top of the pipe. The scaling of the shear stresses is not affected, however, since the wall shear stress in single-phase flow of both fluid g and l are given by (55a) in horizontal or friction dominated flow in which $B_g = B_l$.

7.3. Inclined flow and the two-phase gravity effect

The non-dimensional horizontal or friction dominated flows, discussed in the previous section, are for a given holdup, completely determined by the viscosity ratio η_g/η_l. Generally, however, in inclined pipes the driving force ratio B_l/B_g must also be considered, see Section 7.1. In single-phase flow a change in the pipe inclination (for a given holdup) simply alters the driving force, leaving the corresponding non dimensionalized flow unchanged. In two-phase flow, however, there is an additional *two-phase gravity effect* given by the deviation of the driving force ratio from unity in inclined pipes — i.e. the value of $1 - B_l/B_g$. The two-phase gravity effect thus represents the departure from the conditions in horizontal or friction dominated flow in an inclined pipe. We have $\rho_g/\rho_l \leq 1$ by definition. The two-phase gravity effect is zero in the special case that $\rho_g/\rho_l = 1$ for which $B_l/B_g \equiv 1$, and increases as the density ratio ρ_g/ρ_l decreases. The two-phase gravity effect is large, for a given holdup, if the body force in the more dense fluid l is comparable to the pressure gradient — i.e. if $|\rho_l g \sin\theta/(\partial p/\partial z)| \sim O(1)$. It decreases, however, as the pressure gradient increases or the pipe angle θ decreases. In order to simplify the discussion we will only consider cases involving very low or high viscosity ratios. We will also, without further loss of generality, assume that the driving force in fluid g works in the positive z-direction i.e. that $-B_g > 0$, implying that $B_l/B_g < 1$ and $B_l/B_g > 1$ in up- and downwardly inclined pipes, respectively. (Note that $-B_g > 0$ and e.g. $B_l/B_g < 1$ implies that $B_l > B_g$ or $(\rho_l - \rho_g)g \sin\theta > 1$ i.e. $\theta > 0$.) We start with the low viscosity ratio case $\eta_g/\eta_l \ll 1$ typical for gas–liquid flows.

The limiting behaviour of the mean wall and interfacial shear stresses for very low viscosity ratios ($\eta_g/\eta_l \to 0$) may be obtained by neglecting all terms proportional to η_g/η_l in Eqs. (56)–(58). The resulting expressions are thus independent of the viscosity ratio, and given by

$$\frac{\bar{\tau}_g}{\tau_g^s} \approx 1 - \frac{\sin^2 \delta_g}{\delta_g^2} \tag{59}$$

$$\frac{\bar{\tau}_l}{\tau_g^s} \approx 1 + \frac{\sin^2 \delta_l}{\delta_g \delta_l} - \left(1 - \frac{B_l}{B_g}\right)\left(\frac{\delta_l - \frac{1}{2}\sin 2\delta_l}{\delta_l}\right) \tag{60}$$

$$\frac{\bar{\tau}_i}{\tau_g^s} \approx \frac{\sin\delta_g - \delta_g\cos\delta_g}{\delta_g} \tag{61}$$

Studying Eqs. (59)–(61) we see that the two-phase gravity effect $(1 - B_l/B_g)$ is only present in the expression (60) for the mean wall shear stress in the more viscous (and dense) fluid l. It does not enter into the expressions for the mean wall shear stress in fluid g (59) or interfacial shear stress (61). This observation simply reflects the fact that the limit $\eta_g/\eta_l \to 0$ corresponds to a physical situation in which the less viscous (and dense) fluid g is flowing as in single-phase closed duct flow above an infinitely more viscous and slower (frozen) fluid l. Fluid g is thus only affected by the two-phase flow situation through the holdup (δ_g) defining the "duct" geometry. This is thus also the situation for the shear stress — wall and interfacial — as seen by fluid g. The more viscous fluid l, however, is highly dependent on the interfacial drag exerted by infinitely faster fluid g, and is thus more directly influenced by the two-phase flow situation. Fig. 3 gives us an idea of how small the viscosity ratio η_g/η_l must be for the Eqs. (59)–(61) to be good approximations. It is seen that the results for $\eta_g/\eta_l = 0.01$ are very close to the limiting values $\eta_g/\eta_l \to 0$ (dash dot lines), provided that the holdup is not too high. The maximum discrepancy in any of the shear stresses is $\approx 2\%$ i.e. $O(\eta_g/\eta_l)$ for $\delta_l < \pi/2$.

Fig. 5 displays the approximate mean wall shear stress (59)–(61) for $0 \le \delta_l/\pi \le 1$. The left hand plot in Fig. 5 contains a comparison for *horizontal* or friction dominated flow.The dashed line represents the mean duct shear stress (wall and interfacial) as seen by the less viscous fluid g — i.e. the value of $(\bar{\tau}_g S_g + \bar{\tau}_i S_i)/(S_g + S_i)$. The mean wall shear stress in fluid g is seen to be lower than this value for all holdup. The mean interfacial shear stress on the other hand is always higher. The maximum deviations are $\approx -3\%$ and $\approx +8.2\%$, respectively. The deviations are caused by the non-circularity of the cross section occupied by fluid g. The mean wall shear stress in fluid l is seen to reach a maximum for $\delta_l = \pi/2$ in horizontal or friction dominated flow. It is then, as mentioned in the previous section, $\approx$ 41% higher than in single-phase flow (unity).

As discussed above, the non dimensional wall shear stress in the less viscous fluid g and the interfacial shear stress are unaffected by a pipe inclination and the two-phase gravity effect in the low viscosity limit $\eta_g/\eta_l \to 0$. The mean wall shear stress in the more viscous fluid l is, however, highly influenced, as may be observed in the right hand plot in Fig. 5. The plot shows how the two-phase gravity effect causes the mean wall shear stress in fluid l to decrease in upwardly inclined pipes $B_l/B_g < 1$ (thin solid lines) and increase in downwardly inclined pipes $B_l/B_g > 1$ (dashed lines) — as the body forces oppose or work in the direction of the flow respectively. The two-phase gravity effect decreases as the holdup decreases and the interfacial drag becomes increasingly important. This phenomenon is connected to the fact that the flow area A_l — acted upon by the driving force B_l — vanishes in the zero holdup limit, whereas the interfacial to wetted perimeter ratio S_i/S_l becomes unity. (Note that: $A_l/A = \epsilon_l \approx 2\delta_l^3/(3\pi)$ whereas $S_i/S_l \approx 1$ as $\delta_l \to 0$, by Eqs. (9) and (42).

Fig. 6 shows the wall and interfacial shear stress distributions (33) and (26) corresponding to the mean values in Fig. 5 for $\delta_l = \pi/4, \pi/2$ and $3\pi/4$. The velocity and shear stress profiles on the vertical symmetry line of the pipe, as given by Eqs. (28) and (31) with $\xi = 0$, are also shown. The shear stress in Fig. 6 is scaled by Eq. (55b), as in Figs. 3–5. Scaling the velocity by ((55a)), as in Fig. 4, however, causes the velocity in fluid g to collapse onto the single-phase

closed duct flow profile, irrespective of driving force ratio. The dimensionless velocity in fluid l, on the other hand, becomes zero in the limit $\eta_g/\eta_l \to 0$ (see corresponding (dash dot) velocity profiles for $\eta_g/\eta_l \to 0$). We are now, however, interested in the two-phase gravity effect in fluid l. The velocity profiles in Fig. 6. have therefore been scaled by the special parameter $U_m = -B_g R^2/8\mu_l$ — i.e. the mean single-phase velocity corresponding to a viscosity η_l and driving force B_g. This scaling magnifies the events in fluid l as well as in fluid g. The velocity distribution in the infinitely faster moving fluid g, is thus not contained in the plots.

The thick solid lines in Fig. 6. correspond to horizontal or friction dominated flow, whereas the thin solid and dashed lines correspond to gravity influenced up- and downwardly inclined flows, respectively — as in the right-hand plot in Fig. 5. The collapsing of shear stress distributions from the interface and up reflects the absence of the two-phase gravity effect in fluid g, in agreement with the single-phase closed duct flow behaviour for $\eta_g/\eta_l \to 0$. The two-phase gravity effect is, however, evident in fluid l, which is highly influenced by the infinitely faster moving fluid g. This is clearly seen in the corresponding spread in the velocity and shear stress distributions below the interface.

Fluid l is in pure shear flow when the body forces are exactly balanced by the pressure gradient i.e. $B_l/B_g = 0$, see velocity and shear stress distributions marked ($\otimes$). For $B_l/B_g < 0$ the net driving force in fluid l will be directed down the pipe, since by assumption $-B_g > 0$. In this case, backflow may occur, starting at the bottom of the pipe, provided that the holdup is sufficiently high for the body force to overcome the combined action of the pressure gradient and the interfacial drag. Backflow may be observed in the velocity profiles corresponding to $B_l/B_g < 0$ and $\delta_l = \pi/2$ and $3\pi/4$ in Fig. 6 — i.e. to the left of the pure shear flow profiles marked ($\otimes$). The backflow is accompanied by corresponding negative local values in the wall shear stress distribution. The mean wall shear stress, displayed in the right hand plot in Fig. 5,

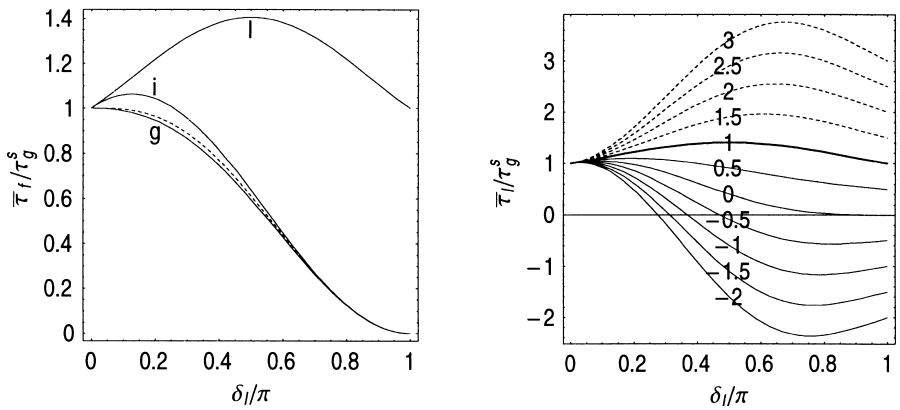

Fig. 5. Dimensionless mean wall and interfacial shear stress (56)–(58) for $\eta_g/\eta_l = 0$ as given by Eqs. (59)–(61). Left-hand plot: comparison for horizontal or friction dominated flow $B_l/B_g = 1$. Dashed line: mean shear stress (wall and interfacial) as seen by the less viscous fluid g. Right-hand plot: two-phase gravity effect in the wall shear stress in fluid l. Thick solid line: horizontal or friction dominated flow $B_l/B_g = 1$. Thin dashs lines: downwardly inclined gravity influenced flows $B_l/B_g = 1.5, 2, 2.5, 3$. Thin lines: upwardly inclined gravity flows $B_l/B_g = -2, -1.5, -1, 0.5, 0, 0.5$.

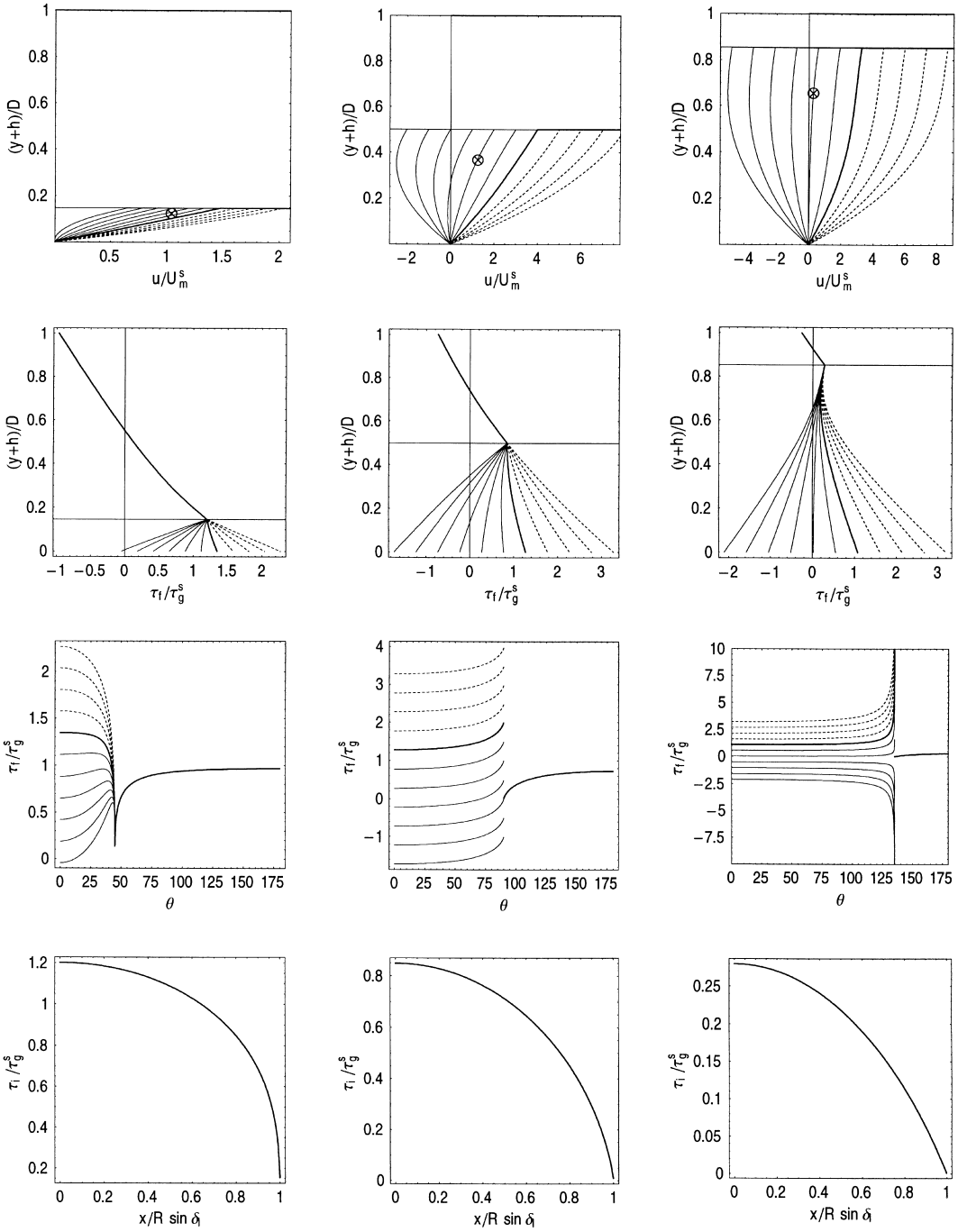

Fig. 6. Velocity and shear stress distributions for up and downward inclined gravity influenced flow in the limit $\eta_g/\eta_l \to 0$. Top two rows: velocity and shear stress distributions on vertical symmetry line. Bottom rows: wall and interfacial shear stress. Columns left to right: $\delta_l = \pi/4, \pi/2, 3\pi/4$. Thick solid line: horizontal or friction dominated flow wall and interfacial shear stress Columns left to right: $\delta_l = \pi/4, \pi/2, 3\pi/4$. Thick solid line: horizontal or friction dominated flow $B_l/B_g = 1$. Thin dashed lines: downwardly inclined gravity influenced flows $B_l/B_g = 1.5$, 2, 2.5, 3. Thin lines upwardly inclined gravity influenced flows $B_l/B_g = -2$, -1.5, -1, 0.5, 0, 0.5.

will eventually also become negative as the backflow increases and spreads towards the interface.

The viscosity ratio may be very large $\eta_g/\eta_l \gg 1$ in two-phase flows involving e.g. a highly viscous oil on top of water. By symmetry the inclined flow case for a very high viscosity ratio $\eta_g/\eta_l \to \infty$ (or $\eta_l/\eta_g \to 0$) may be studied by simply holding Fig. 6 upside-down. Now, assuming that $-B_l > 0$, the dashed lines correspond to upwardly inclined flows i.e. $B_g/B_l > 1$, whereas the thin solid lines correspond to downwardly inclined flows or $B_g/B_l < 1$. It must also be understood that the velocity in the now *more* viscous (but still less dense) fluid g is scaled by $U_m = -B_l R^2/8\mu_g$, and that the shear stress is scaled by the single-phase value in the more dense fluid $\tau_l = -B_l R/2$. The remaining changes are the same as in the similar study using Fig. 4, discussed at the end of Section 7.2. Holding Fig. 6 upside down displays the two-phase gravity effect in the less dense fluid g in the high viscosity ratio limit $\eta_g/\eta_l \to \infty$ for which the more dense fluid l behaves as in single-phase closed duct flow. In this situation the wall shear stress in fluid g *decreases* in downwardly inclined flow due to the static head of fluid l, which eventually forces fluid g to backflow *up* the pipe. (Note that the positive flow direction is now from right to left). The situation is reversed in an upwardly inclined pipe, for which the static head of fluid l causes the wall shear stress in fluid g to increase.

8. Conclusion

The basic solution for pressure driven two-phase laminar stratified pipe flow (33) has been recast into a simpler form, alleviating its physical interpretation and constituting a more convenient basis for further developments. The simplifications are facilitated by placing the (bipolar) coordinate axes on the interface and vertical symmetry line of the pipe, respectively. This reference frame emphasizes the natural two-phase symmetry and allows us to write the solution for the phases $f = g$ and l as one generic expression for the general phase f. A further structuring is given by the special definition (22), which enables us to split the solution into a single-phase free surface flow term and a two-phase interfacial drag coupling term.

The corresponding expression for the interfacial shear stress distribution (26) now emerges naturally as a consequence of the no-slip condition on the interface in complete analogy with the situation in the corresponding channel flow problem, solved in Appendix A. The wall shear stress distributions (33) are obtained by formal differentiation. The general behaviour of the wall and interfacial shear stresses in the triple points, where the fluid–fluid interface meets the pipe wall, are given by application of residue calculus as summarized in Section 5. The highly organized equations developed here lead directly to the new and surprisingly simple expression for the mean interfacial shear stress (48) representing the local solution of the boundary value problem at the interface. This expression complements the fluid momentum balances (54) and facilitates the simple computation of the exact general solution for the mean wall and interfacial shear stresses for a given holdup and pressure drop in a given pipe containing a given pair of fluids. The recast laminar flow solution developed here reduces identically to the solution for a single fluid f subject to a *constant* surface shear stress distribution, as studied in Biberg (1999b), by a simple substitution, see discussion at the beginning of Section 7. Some

applications of the laminar flow theory to 1D turbulent flow modelling are given in Biberg (1999a).

Acknowledgements

The work presented here was supported by the Norwegian state oil company STATOIL A/S. It has previously been presented in part at the informal workshop: *European Two-phase Flow Group Meeting* in Den Bosch, Holland 30 May - 2 June 1995.

Appendix A. Channel flow

We introduce the Cartesian coordinates (y, z) and let the z-axis point in the direction of flow and the fluid–fluid interface and channel walls be defined by $y = 0$ and $y = \pm h_f$, respectively. The z-components of the Navier–Stokes equations in the channel are given by

$$\frac{\partial^2 u_f}{\partial y^2} = \frac{B_f}{\eta_f} \tag{A1}$$

The boundary conditions are the no-slip conditions on the channel walls and interface, given by

$$u_f\big(y = \pm h_f\big) = 0 \tag{A2a}$$

$$u_g(y = 0) = u_l(y = 0) \tag{A2b}$$

respectively, and continuous shear stress condition on the interface, given by

$$\eta_f \frac{\partial u_f}{\partial y}(y = 0) = \tau_i \tag{A3}$$

Solving Eqs. (A1)–(A3) yields the solution for the velocity field, given by

$$u_f = -\overbrace{\frac{B_f h_f^2}{2\eta_f}\left[1 - \left(\frac{y}{h_f}\right)^2\right]}^{\text{free surface flow}} \mp \overbrace{\frac{\tau_i h_f}{\eta_f}\left(1 \mp \frac{y}{h_f}\right)}^{\text{shear flow}} \tag{A4}$$

in which the no-slip condition on the interface (A2b) determines the interfacial shear stress as

$$\tau_i = \frac{\eta_g B_l h_l^2 - \eta_l B_g h_g^2}{2\big(\eta_g h_l + \eta_l h_g\big)} \tag{A5}$$

Introducing Eq. (3) and the channel flow phase fractions $\epsilon_f = h_f/H$ where $H = h_g + h_l$ in Eq. (A5), yields the alternative form

$$\tau_i = \frac{H}{2\left(\eta_g \epsilon_l + \eta_l \epsilon_g\right)}\left[\eta_g\left(\frac{\partial p}{\partial z} + \rho_l g \sin\theta\right)\epsilon_l^2 - \eta_l\left(\frac{\partial p}{\partial z} + \rho_g g \sin\theta\right)\epsilon_g^2\right] \tag{A6}$$

The shear stress in the z-direction (direction of flow) on a surface $y = \text{constant}$, is given by

$$\tau_{f,\,y,\,z} = \eta_f \frac{\partial u_f}{\partial y} = B_f y + \tau_i \tag{A7}$$

Following the definitions in Fig. 1, the wall shear stresses are thus given by

$$\tau_f = \mp \tau_{f,\,y,\,z}\left(y = \pm h_f\right) = -B_f h_f \mp \tau_i \tag{A8}$$

using Eq. (A4). Introducing Eq. (3) shows that (A8) are equivalent to the fluid momentum balances in the channel, given by

$$h_f\left(\frac{\partial p}{\partial z} + \rho_f g \sin\theta\right) + \tau_f \pm \tau_i = 0 \tag{A9}$$

Appendix B. Triple point analysis

The behaviour of the wall and interfacial shear stresses (33) and (26) in the triple points where the interface meets the pipe wall, is given by the limits $\xi \to \pm\infty$. Due to symmetry, however, it suffices to consider e.g. $\xi \to \infty$. The wall shear stress distribution (33) may be written as

$$\tau_f = -\frac{B_f R}{2} + \left(\cosh\xi + \cos\delta_f\right)\int_{-\infty}^{\infty} \frac{\Psi_f(\omega)\omega e^{i\omega\xi}}{\sinh\omega\pi\cosh\omega\delta_f}\,d\omega \tag{B1}$$

in which we have introduced complex notation and defined

$$\Psi_f(\omega) = \frac{B_f R\cos\delta_f}{2} \mp \mathscr{T}_i(\omega) \tag{B2}$$

inserting $\mathscr{T}_i(\omega)$ from Eq. (25), we find that $\Psi_g(\omega) = \Phi_{gl}(\omega)$ and $\Psi_l(\omega) = \Phi_{lg}(\omega)$ where

$$\Phi_{gl}(\omega) = \frac{R}{2}\left[\frac{\left(\eta_l B_g - \eta_g B_l\right)\omega\sin\delta_g + \eta_g\left(B_g - B_l\right)\cos\delta_g \tanh\omega\delta_l}{\eta_g\tanh\omega\delta_l + \eta_l\tanh\omega\delta_g}\right] \tag{B3}$$

The integral in Eq. (B1) tends to zero as $\xi \to \infty$. The factor $\cosh\xi \sim e^{\xi}/2$, however, tends to infinity. The limiting behaviour of the wall shear stress (B1) is thus contained in

$$\tau_f(\xi \to \infty) = -\frac{B_f R}{2} + \frac{e^{\xi}}{2}\int_{-\infty}^{\infty} \frac{\Psi_f(\omega)\omega e^{i\omega\xi}}{\sinh\omega\pi\cosh\omega\delta_f}\,d\omega \tag{B4}$$

Following a similar line of reasoning starting with Eq. (26), we find that the limiting behaviour of the interfacial shear stress is contained in

$$\tau_i(\xi\to\infty) = \frac{e^{\xi}}{2}\int_{-\infty}^{\infty} \frac{\mathscr{T}_i(\omega)\omega e^{i\omega\xi}}{\sinh\omega\pi}\,d\omega \tag{B5}$$

Now, applying the residue theorem — choosing the appropriate integration path in the upper half of the complex-ω plane — the leading asymptotic behaviour of the integrals in Eqs. (B4) and (B5) is found to be given by the singularity ω_0 ($\mathrm{Im}(\omega_0) > 0$) of the integrands closest to the real axis. We have

$$\int_{-\infty}^{\infty} \frac{f(\omega)}{g(\omega)} e^{i\omega\xi}\,d\omega \sim 2\pi i \left\{ \begin{array}{l} \dfrac{1}{g'(\omega_0)} \\ \dfrac{2}{g''(\omega_0)}\left(\dfrac{i\xi f(\omega_0) + f'(\omega_0)}{f(\omega_0)} - \dfrac{1}{3}\dfrac{g'''(\omega_0)}{g''(\omega_0)}\right) \end{array} \right\} f(\omega_0)e^{i\omega_0\xi} \tag{B6}$$

in the case of a single and double pole, respectively. The denominators of $\Psi_f(\omega)$ and $T_i(\omega)$ in Eqs. (B4) and (B5) are equal and the zeros on the imaginary-ω axis are given by

$$\eta_g \tan\delta_l v_k + \eta_l \tan\delta_g v_k = 0 \tag{B7}$$

for $k = 1, 2, \ldots$ and $0 < v_0 < v_1 < \cdots$ where $v = \mathrm{Im}(\omega)$. The zeros of the $\sinh\omega\pi$ term in the denominators of the integrands in Eqs. (B4) and (B5) are $\omega = 0, i, 2i, \ldots$. The first zero $\omega = 0$ will, however, be cancelled by the ω-term in the numerators. If $\eta_g/\eta_l > 0$, the zeros of $\cosh\omega\delta_f$ in Eq. (B4) will either be neutralized by the singularities in the denominator of $\Psi_f(\omega)$ or in the case of $\delta_f = \pi/2n$ coincide with a subset of the zeros in $\sinh\omega\pi$. The case $\eta_g/\eta_l = 0$, must be considered separately.

- *Case* 1: $\eta_g/\eta_l < 1$ and $\delta_l < \pi/2$. In this case, $v_0 > 1$ and thus $\omega_0 = i$. Eq. (25) yields $\mathscr{T}_i(\omega = i) = 0$ for $\eta_g/\eta_l < 1$. Combining Eqs. (B2) and (B4) thus yields

$$\tau_f(\xi\to\infty) = -\frac{B_f R}{2} + \frac{B_f R\cos\delta_f}{2}\frac{e^{\xi}}{2}\int_{-\infty}^{\infty} \frac{\omega e^{i\omega}}{\sinh\omega\pi\cosh\omega\delta_f}\,d\omega \tag{B8}$$

  Applying Eq. (B6) (for a single pole) we find that the integral in Eq. (B8) behaves as $\sim 2e^{-\xi}/\cos\delta_f$. We thus have $\tau_f(\xi\to\infty) = 0$. The singularity $\omega_0 = i$ will not contribute to the asymptotic behaviour of the interfacial shear stress (B5) since $\mathscr{T}_i(\omega = i) = 0$. We must therefore either consider $\omega = 2i$ or $\omega = iv_0$ if $v_0 < 2$. The corresponding leading behaviours of the integral in Eq. (B5) are $O(e^{-2\xi})$ or $O(e^{-v_0\xi})$, respectively. We thus also have $\tau_i(\xi\to\infty) = 0$ in this case.
- *Case* 2: $\eta_g/\eta_l < 1$ and $\delta_l = \pi/2$ $(= \delta_g)$. As in Case 1, we have $v_0 > 1$ and $\omega_0 = i$. Inserting $\delta_g = \delta_l = \pi/2$ in Eqs. (B4) and (B5), however, yields

$$\tau_f(\xi\to\infty) = -\frac{B_f R}{2} \mp \frac{(\eta_g B_l - \eta_l B_g)R}{2(\eta_g + \eta_l)}\frac{e^{\xi}}{2}\int_{-\infty}^{\infty} \frac{\omega^2 e^{i\omega\xi}}{\sinh\omega\pi\sinh(\omega\pi/2)}\,d\omega \tag{B9}$$

  and

$$\tau_i(\xi\to\infty) = \frac{(\eta_g B_l - \eta_l B_g)R}{4(\eta_g+\eta_l)}\frac{e^{\xi}}{2}\int_{-\infty}^{\infty}\frac{\omega^2 e^{i\omega\xi}}{\sinh^2(\omega\pi/2)}\,d\omega \tag{B10}$$

Applying Eq. (B6) for a single pole with $\omega_0 = i$, we find that the integral in Eq. (B9) behaves as $\sim 2e^{-\xi}$ yielding the limiting behaviour for the wall shear stresses as given by Eq. (35). There are double poles in Eq. (B10). The closest singularity contributing to the integral is $\omega = 2i$. Applying Eq. (B6) we find that the integral in Eq. (B10) behaves as $\sim(32/\pi)\times(\xi-1)e^{-2\xi}$ and consequently that $\tau_i(\xi\to\infty) = 0$.

- *Case* 3a: $0 < \eta_g/\eta_l < 1$ and $\delta_l > \pi/2$. In this case, $v_0 < 1$ and $\omega_0 = v_0 i$. The first term in Eq. (B2) will not contribute to the asymptotic behaviour of the wall shear stress (B4). Applying Eq. (B6) to Eqs. (B4) and (B5) yields the limiting behaviour for the wall and interfacial shear stress as given by Eq. (37) in Section 5, in which

$$K = \frac{\pi R v_0}{2\sin\pi v_0}\left[\frac{\eta_g B_l(v_0\sin\delta_l - \cos\delta_l\tan(\delta_l v_0)) - \eta_l B_g\left(v_0\sin\delta_g - \cos\delta_g\tan\left(\delta_g v_0\right)\right)}{\delta_l\eta_g\sec^2(\delta_l v_0) + \delta_g\eta_l\sec^2\left(\delta_g v_0\right)}\right] \tag{B11}$$

The absolute value sign on the $\cos(\delta_f v_0)$-term in Eq. (37) takes care of the fact that $\pm\cos(\delta_f v_0) > 0$. (Note that Eq. (B7) implies that $\eta_g\tan(\delta_l v_0) = -\eta_l\tan(\delta_g v_0) < 0$ since $\delta_g = \pi - \delta_l < \pi/2$ and $0 < v_0 < 1$.) It may be demonstrated that the sign of constant (B11) is given by

$$\mathrm{sign}(K) = \mathrm{sign}\left[\frac{\eta_g}{\eta_l}B_l - Bg - \left(B_l - B_g\right)k_1\right] \tag{B12}$$

in which $k_1 = \tan(\delta_g v_0)/(v_0\tan\delta_g)$ and $0 < k_1 < 1$.

- *Case* 3b: $\eta_g/\eta_l = 0$ and $\delta_l > \pi/2$. If $f = g$ in Eq. (B4), then $\omega_0 = i$ as in Case 1, and consequently $\tau_g(\xi\to\infty) = 0$. Similarly, we also have $\tau_i(\xi\to\infty) = 0$. If $f = l$, however, then $\omega_0 = \pi i/2\delta_l$ in Eq. (B4) yielding $\sim\pi^2 e^{(-\pi^2\xi/2\delta_l)}/\delta_l^2\sin(\pi^2/2\delta_l)$ for the integral by application of Eq. (B6), and thus that $\tau_l(\xi\to\infty) = \infty$.
- *Equal viscosity case*: $\eta_g/\eta_l = 1$. We start by considering $\delta_l < \pi/2$, for which $\omega_0 = i$. If $\eta_g/\eta_l \neq 1$, $\mathscr{T}_i(\omega\to i) = 0$. Now, however, we have the non zero limit, given by

$$\lim_{\omega\to i}\mathscr{T}_i(\omega) = -\frac{R\cos\delta_l}{2}\left(B_g\epsilon_g + B_l\epsilon_l\right)\quad\text{for } \eta_g/\eta_l = 1 \tag{B13}$$

where ϵ_f are given by Eq. (9). Applying Eq. (B6) to Eqs. (B4) and (B5) using Eqs. (B13) and (B2) yields the finite limits for the wall and interfacial shear stresses as given by Eq. (40) in Section 5. These limits do in fact apply for $\eta_g/\eta_l = 1$ irrespective of holdup i.e. δ_l: If $\delta_l = \pi/2$, we obtain the identical result as given by Eq. (40) by simply inserting $\eta_g/\eta_l = 1$ in Case 2 above. (Note that $\epsilon_f = 1/2$ for $\delta_l = \pi/2$ and that the result $\tau_i(\xi\to\infty) = 0$ is contained in Eq. (40) since $\cos(\pi/2) = 0$.) If $\delta_l > \pi/2$, we may establish Eq. (40) by applying Eq. (B6) on Eqs. (B4) and (B5) with $\omega_0 = i$. We may, however, also simply take the limit of Case 3 above for $\eta_g/\eta_l = 1$ and $v_0\to 1$ (the correct solution of Eq. (B7) in this case).

References

Bentwich, M., 1964. Two-phase viscous axial flow in a pipe. J. Basic Eng. (12) 669–672.

Biberg, D., 1999a. Two-phase stratified pipe flow modelling — a new expression for the interfacial shear stress. In: Second International Symposium on Two-Phase Flow Modelling and Experimentation, Pisa (Italy), 23–26 May.

Biberg, D., 1999b. Liquid wall friction in two-phase turbulent gas laminar liquid stratified pipe flow. Can. J. Chem. Eng. 77, 1073–1082.

Biberg, D., 1999c. An explicit approximation for the wetted angle in two-phase stratified pipe flow. Can. J. Chem. Eng. 77, 1221–1224.

Brauner, N., Rovinsky, J., Maron, D.M., 1996a. Analytic solution for laminar-laminar two-phase stratified flow in circular conduits. Chem. Eng. Comm 141/142, 103–143.

Brauner, N., Rovinsky, J., Maron, D.M., 1996b. Determination of the interface curvature in stratified two-phase systems by energy considerations. Int. J. Multiphase Flow 22 (6), 1167–1185.

Charles, M.E., Redberger, P.J., 1962. The reduction of pressure gradients in oil pipelines by the addition of water: numerical analysis of stratified flow. Can. J. Chem. Eng. (4) 70–75.

Charles, M.E., Lilleleht, L.U., 1965. Co-current stratified laminar flow of two immiscible liquids in a rectangular conduit. Can. J. Chem. Eng. (6) 110–116.

Coutris, N., Delhaye, J.M., Nakach, R., 1989. Two-phase flow modelling: the closure issue for a two-layer flow. Int. J. Multiphase Flow 15 (6), 977–983.

Gemmell, A.R., Epstein, N., 1962. Numerical analysis of stratified laminar flow of two immiscible newtonian liquids in a circular pipe. Can. J. Chem. Eng. (10) 215–225.

Joseph, D.D., 1984. Instability of the flow of two immiscible liquids with different viscosities in a pipe. J. Fluid Mech 141, 309–317.

Lightstone, L., Chang, J.S., 1981. Three-dimension stratified laminar gas–liquid two-phase pipe flow models 1991. In: Proc. of the 2nd Int. Symp. on Multiphase Flow and Heat Transfer, Xian (China) 18–2 Sept. 1989, 67–77.

Masliyah, J.H., Shook, C.A., 1978. Two-phase laminar zero net flow in a circular inclined pipe. Can. J. Chem. Eng 56, 165–175.

Packham, B.A., Shail, R., 1971. Stratified laminar flow of two immiscible fluids. Proc. Camb. Phil. Soc 69, 443–448.

Ranger, K.B., Davis, A.M.J., 1979. Steady pressure driven two-phase stratified laminar flow through a pipe. J. Chem. Eng 57, 688–691.

Rosant, J.M., 1986. Mcanique des fluides — Metode de calcul d'un coulement diphasique, stratifi et laminaire, en conduite circulaire. C.R. Acad. Sc. Paris, t. 302, Serie II, no. 5, 197–200.

Semenov, N.I., Tochigin, A.A., 1961. An analytical study of the separate laminar flow of a two-phase mixture in inclined pipes. J. Eng. Phys 4, 29.

Tang, Y.P., Himmelblau, D.M., 1963. Velocity distribution for isothermal two-phase co-current laminar flow in a horizontal rectangular duct. Chem. Eng. Sci 18, 143–144.

Teletov, S.G., 1946. On the slow stratified movement of gas–liquid mixtures. Compt. Rend. Acad. Sci. U.R.S.S 51, 579.

Yu, H.S., Sparrow, E.M., 1967. Stratified laminar flow in ducts of arbitrary shape. A.I.Ch.E. J 13 (1), 11–16.

Yu, H.S., Sparrow, E.M., 1969. Experiments on two-component stratified flow in a horizontal duct. J. Heat Transf., Trans. of the ASME 91, 51–58.